

Gravitational Scattering of Cosmic Strings by Non-Rotating Black Holes. *

Jean-Pierre De Villiers^{†1}, and Valeri Frolov^{‡1,2}

February 5, 2020

¹*Theoretical Physics Institute, Department of Physics, University of Alberta,
Edmonton, Canada T6G 2J1*

²*CIAR Cosmology Program*

Abstract

This paper discusses the gravitational scattering of a straight, infinitely long test cosmic string by a black hole. We present numerical results that probe the two-dimensional parameter space of impact parameter and initial velocity and compare them to approximate perturbative solutions derived previously. We analyze string scattering and loop formation in the ultra-relativistic regime and compare these results with analytical results for string scattering by a gravitational shock wave. Special attention is paid to regimes where the string approaches the black hole at near-critical impact parameters. The dynamics of string scattering in this case are highly sensitive to initial data and transient phenomena arise while portions of the string dwell in the strong gravitational field near the event horizon of the black hole. The role of string tension is also investigated by comparing the scattering of a cosmic string to the scattering of a tensionless "dust" string. Finally, the problem of string capture is revisited in light of these new results, and a capture curve covering the entire velocity range ($0 < v \leq c$) is given.

PACS number(s): 04.60.+n, 12.25.+e, 97.60.Lf, 11.10.Gh

*Preprint Alberta Thy 08-98

[†]e-mail: jpd@phys.ualberta.ca

[‡]e-mail: frolov@phys.ualberta.ca

1 Introduction

In this paper we study the interaction of a cosmic string with a (non-rotating) black hole. This problem is interesting for many reasons. First of all, it is a rare example of gravitational interaction between two extended relativistic objects that allows complete analysis. When a cosmic string comes close to a black hole and is captured by it, one might expect generation of strong gravitational radiation, which makes the problem potentially interesting for astrophysical applications. Besides this, the study of the interaction of a cosmic string with a black hole has demonstrated some unexpected, physically interesting possibilities, such as the creation of 2D black holes [1].

For astrophysically interesting cases, the dimensionless parameter $\mu^* = G\mu/c^2$, where μ is the string tension, is small. For example, for strings formed during a GUT phase transition, $\mu^* \approx 10^{-5}$. For this reason, in the leading order one can neglect gravitational backreaction effects and consider the string as a test object propagating in a given gravitational background. The worldsheet of such a string is a minimal surface which gives an extremum to the Nambu-Goto action [2].

Stationary configurations of a cosmic string in the field of a rotating charged black hole are described by worldsheets which are tangent to the Killing vector generating the time shift. Because of this symmetry, the problem is reduced to finding a geodesic in a three-dimensional space; the latter can be solved by separation of variables [3]. In the absence of such a symmetry, non-linear partial differential equations describing the string motion in the gravitational field of the black hole do not allow exact solutions. Under these conditions one either needs approximation schemes or numerical solutions. In the present paper we assume that the string is initially far from the non-rotating black hole, straight, and moving with velocity v in the direction of the black hole. The motion of the string is affected by the gravitational field of the black hole. For a given velocity v , the outcome of the interaction depends on the impact parameter b . If the impact parameter is large enough, the string escapes the gravitational attraction of the black hole and is inelastically scattered. For smaller values of b the string is captured by the black hole.

The scattering of a cosmic string for very large impact parameters was studied in [4, 5]. Such a string passes far from the black hole and its motion is modified only slightly. Under these conditions one can consider the gravitational interaction as a perturbation and treat it by expanding the solution in powers of the Newtonian gravitational potential $\varphi = GM/(Rc^2)$. The numerical study of string scattering by a black hole was initiated by Moss and Lonsdale [6]. In Ref. [7] we used numerical calculations to obtain

the dependence of the critical capture impact parameter on velocity v , and demonstrated that the results of Moss and Lonsdale do not correctly reproduce the behaviour of the critical impact parameter at high velocities.

In order to obtain more detailed information on the characteristics of scattering and capture of a cosmic string by a black hole we performed further numerical calculations. In regimes that allow analytical study, we compared numerical and analytical results. The agreement of these results was used as an additional test of our calculations. We also analysed the role of tension in the string by comparing the relativistic string results with those for a string without pressure (a so-called “dust model”). These results are discussed in the following sections. In Section 2 we formulate the scattering problem for the straight string. Section 3 outlines the numerical method that was used and discusses the scattering at shallow impact parameters. It also contains comparison of these results with the results obtained in the weak-field approximation. Section 4 compares numerical and approximate analytical results for a string moving with ultra-relativistic velocity. It also discusses loop formation for the scattering in this regime. Section 5 discusses near-critical scattering, where the string worldsheet is partially wrapped around the black hole. Section 6 discusses the role played by the tension of the string and makes a comparison with the model of a dust string. Section 7 discusses aspects of the problem connected with string capture.

2 Scattering Problem for a Straight String

2.1 Equations of motion

The two-dimensional worldsheet representing a moving string is parametrized as $\mathcal{X}^\mu(\zeta^A)$; \mathcal{X}^μ ($\mu = 0, 1, 2, 3$) are the spacetime coordinates, and ζ^A ($A = 0, 3$) are the worldsheet coordinates $\zeta^0 = \tau$, $\zeta^3 = \sigma$. The equations of motion of the string follow from the Nambu-Goto action [8] which we write in the Polyakov form [2]

$$I[\mathcal{X}, h] = -\frac{\mu}{2} \int d\tau d\sigma \sqrt{-h} h^{AB} G_{AB}. \quad (2.1)$$

We use units in which $G = c = 1$, and the sign conventions of [9]. In (2.1) h_{AB} is the internal metric with determinant h , and G_{AB} is the induced metric on the worldsheet,

$$G_{AB} = g_{\mu\nu} \frac{\partial \mathcal{X}^\mu}{\partial \zeta^A} \frac{\partial \mathcal{X}^\nu}{\partial \zeta^B} = g_{\mu\nu} \mathcal{X}^\mu_{,A} \mathcal{X}^\nu_{,B}, \quad (2.2)$$

where $g_{\mu\nu}$ is the spacetime metric.

The equations obtained by varying action (2.1) with respect to \mathcal{X}^μ and h_{AB} are of the form

$$\square \mathcal{X}^\mu + h^{AB} \Gamma_{\alpha\beta}^\mu \mathcal{X}_{,A}^\alpha \mathcal{X}_{,B}^\beta = 0 \quad (2.3)$$

and

$$G_{AB} - \frac{1}{2} h_{AB} h^{CD} G_{CD} = 0, \quad (2.4)$$

where $\square = (-h)^{-1/2} \partial_A [(-h)^{-1/2} h^{AB} \partial_B]$. Equations (2.3) are the dynamical equations for string motion, while equations (2.4) are constraints.

2.2 Straight string motion in flat spacetime

Consider first the motion of a straight cosmic string in the absence of an external gravitational field, that is when $g_{\mu\nu} = \eta_{\mu\nu}$, where $\eta_{\mu\nu}$ is the flat spacetime metric. In Cartesian coordinates (T, X, Y, Z) , $\eta_{\mu\nu} = \text{diag}(-1, 1, 1, 1)$ and $\Gamma_{\alpha\beta}^\mu = 0$, and it is easy to verify that, taking $h_{AB} = \eta_{AB} \equiv \text{diag}(-1, 1)$,

$$\mathcal{X}^\mu = X^\mu(\tau, \sigma) \equiv (\cosh(\beta) \tau, \sinh(\beta) \tau + X_0, Y_0, \sigma) \quad (2.5)$$

is a solution of equations (2.3) and (2.4). This solution describes a straight string oriented along the Z -axis which moves in the X -direction with constant velocity $v = \tanh \beta$. Initially, at $\tau_0 = 0$, the string is found at $\mathcal{X}^\mu(0, \sigma) = (0, X_0, Y_0, \sigma)$, where $Y_0 \equiv b$ is the impact parameter. For definiteness we choose $Y_0 > 0$ and $X_0 < 0$, so that $\beta > 0$.

The two-dimensional surface of the worldsheet of such a string is spanned by vectors

$$e_{(0)}^\mu = X_{,\tau} = (\cosh \beta, \sinh \beta, 0, 0) \quad (2.6)$$

and

$$e_{(3)}^\mu = X_{,\sigma} = (0, 0, 0, 1), \quad (2.7)$$

while the vectors

$$e_{(1)}^\mu = n_1^\mu = (\sinh \beta, \cosh \beta, 0, 0) \quad (2.8)$$

and

$$e_{(2)}^\mu = n_2^\mu = (0, 0, 1, 0) \quad (2.9)$$

are orthogonal to the worldsheet. Vectors $e_{(m)}^\mu$ ($m = 0, 1, 2, 3$) form an orthogonal tetrad.

2.3 String motion in a weak gravitational field

The study of scattering of an infinitely long cosmic string by a non-rotating black hole is most conveniently carried out in isotropic coordinates, (T, X, Y, Z) , for which the Schwarzschild metric has the form

$$ds^2 = -\frac{(1 - M/2R)^2}{(1 + M/2R)^2} dT^2 + \left(1 + \frac{M}{2R}\right)^4 (dX^2 + dY^2 + dZ^2), \quad (2.10)$$

where $R^2 = X^2 + Y^2 + Z^2$. This metric can be written as

$$ds^2 = -(1 - 2\Phi)dT^2 + (1 + 2\Psi)(dX^2 + dY^2 + dZ^2) \quad (2.11)$$

with

$$\Phi = \frac{\varphi}{(1 + \frac{1}{2}\varphi)^2} \quad (2.12)$$

and

$$\Psi = \varphi + \frac{3}{4}\varphi^2 + \frac{1}{4}\varphi^3 + \frac{1}{32}\varphi^4, \quad (2.13)$$

where $\varphi = M/R$ is the Newtonian potential.

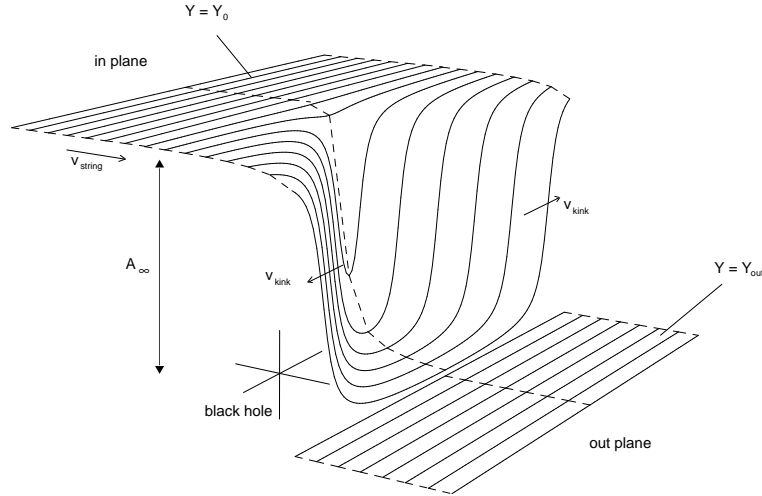


Figure 1: A straight cosmic string scattered by a Schwarzschild black hole.

The motion of the string in the region with small φ can be written in the form

$$\mathcal{X}^\mu(\tau, \sigma) = X^\mu(\tau, \sigma) + \delta X^\mu(\tau, \sigma). \quad (2.14)$$

The straight string starts its motion in the plane $Y = Y_0 = b$. We call it “in-plane” (see Figure 1). This plane represents the motion of the free string in flat spacetime. Deflection of the string worldsheet from the “in-plane”, δX^μ , can be decomposed in the orthogonal frame as

$$\delta X^\mu = \chi^{(m)} e_{(m)}^\mu. \quad (2.15)$$

By linearizing string equations (2.3) and (2.4) one gets the following equations for the first-order perturbations $\chi^{(m)}$ [4]:

$$\square \chi_{(m)} = \left(-\frac{\partial^2}{\partial \tau^2} + \frac{\partial^2}{\partial \sigma^2} \right) \chi_m = f_m, \quad (2.16)$$

where

$$f_{(0)} = 2 \sinh \beta \cosh^2 \beta \varphi_{,X}, \quad (2.17)$$

$$f_{(1)} = 2 \sinh^2 \beta \cosh \beta \varphi_{,X}, \quad (2.18)$$

$$f_{(2)} = -2 \sinh^2 \beta \varphi_{,Y}, \quad (2.19)$$

and

$$f_{(3)} = -2 \cosh^2 \beta \varphi_{,Z}. \quad (2.20)$$

The solutions of linearized equations (2.16)–(2.20) were obtained and analyzed in [4]. Here we reproduce only a solution for $\chi_{(2)}$ which describes the deflection of the string in Y -direction, that is in the spatial direction perpendicular to the string motion. We assume that a straight string starts its motion with $\chi_{(2)} = 0$ at $X_0 = -\infty$ then

$$\chi_{(2)}(\tau, \sigma) = -M \sinh \beta [H_+(\tau, \sigma) + H_-(\tau, \sigma)], \quad (2.21)$$

where

$$H_{\pm}(\tau, \sigma) = \arctan \left[\frac{Y_0^2 + (X_0 + \tau \sinh \beta)(X_0 + s_{\pm} \sinh \beta)}{Y_0 \sinh \beta R(\tau, \sigma)} \right] - \arctan \left[\frac{X_0(X_0 + s_{\pm} \sinh \beta) + Y_0^2}{Y_0 \sinh \beta \sqrt{\rho^2 + s_{\pm}^2}} \right]. \quad (2.22)$$

We use the notation $R^2(\tau, \sigma) = (X_0 + \tau \sinh \beta)^2 + Y_0^2 + \sigma^2$, $\rho^2 = X_0^2 + Y_0^2$, and $s_{\pm} = \tau \pm \sigma$.

The analysis of the late time asymptotic of this solution shows that the string approaches the plane $Y = Y_{out}$, and the shift in position of the string is given by ¹

$$A_{\infty} = Y_0 - Y_{out} = 2M \pi \sinh \beta = 2M \pi \gamma v, \quad (2.23)$$

where $\gamma = (1 - v^2)^{-1/2}$. The late-time solution is represented by a kink and anti-kink, propagating in opposite directions at the speed of light, and leaving behind them the string in a new “phase”. Furthermore, it can be shown that each kink has a characteristic width in the external spacetime given by ²

$$w = \pi Y_0 \coth \beta = \pi \frac{Y_0}{v}. \quad (2.24)$$

¹When $v \rightarrow 0$ second order corrections become important (see [4, 5]). We do not consider the case of extremely slow motion of strings in this paper and always assume that $v > 0.01c$.

²Note that there is an additional factor of π in the expression for the width of the kinks which was absent in [4].

2.4 Scattering data

The above results were obtained under the assumption that the string always propagates in the region where the gravitational field remains weak. In what follows, we describe results concerning string scattering in the regime where the gravitational field cannot be considered weak. Nevertheless, if the string is not captured it eventually emerges from the strong field region and its subsequent evolution is described again by equations (2.16). The string's late time features are characterized by the amplitude A_∞ and width w of the kinks; we refer to these two parameters as the *scattering data*. As will be seen in the following sections, the breakdown of the weak field approximation manifests itself in two ways: the failure of the analytical expressions to correctly reproduce transient shapes, which develop when the string reaches periastron, and discrepancies in the late-time features of the string, namely the scattering data.

3 Strong Field Scattering

3.1 Numerical methods

In order to study the scattering problem under strong-field conditions (where the weak-field approximation breaks down), a numerical solution to the equations of motion must be found. To deal with an infinite cosmic string numerically, a finite computational domain is required, so a method of truncating the string to a reasonably short segment is needed. Such a physical truncation imposes special boundary conditions since it is crucial to reproduce the motion of an infinitely long string with sufficient accuracy.

Two methods of truncating a string were developed. The first places a massive particle at each end of the segment of string and requires that the motion of these particles mimic the motion of the portions of the string lying outside the region of interest. This is accomplished by letting the mass of the end particles go to infinity. The second method places the truncation points a reasonable distance away from the region of interest, subject to the condition that the end points remain in a weak gravitational field where a perturbative solution to the equations of motion is applicable. The analytic weak-field solution is used to prescribe the motion of the boundary points of the string. Each method has distinct advantages, and both were used extensively. Further, the solvers were tested against one another and agreement under identical initial conditions served as an additional validation of the numerical schemes.

With the choice of internal metric $h_{AB} = e^{2\Omega}\eta_{AB}$, the equations of motion have the form

$$\frac{\partial^2 \mathcal{X}^\mu}{\partial \tau^2} - \frac{\partial^2 \mathcal{X}^\mu}{\partial \sigma^2} + \Gamma_{\rho\eta}^\mu \left(\frac{\partial \mathcal{X}^\rho}{\partial \tau} \frac{\partial \mathcal{X}^\eta}{\partial \tau} - \frac{\partial \mathcal{X}^\rho}{\partial \sigma} \frac{\partial \mathcal{X}^\eta}{\partial \sigma} \right) = 0. \quad (3.1)$$

The discretization of these equations (described in detail in Ref. [7]) yields a block-tridiagonal system

with which the solution over the entire spatial (σ) grid is obtained by algebraic methods. The boundary conditions, for which $\mathcal{X}^\mu(\tau, \sigma_i) \equiv X_i^\mu$, are imposed by replacing the first and last entries in the block-tridiagonal system by the required expressions.

For infinitely massive end particles at the boundaries the following equations are substituted into the system,

$$\frac{d^2 X_i^\mu}{d\tau^2} + \Gamma_{\rho\eta}^\mu \frac{dX_i^\rho}{d\tau} \frac{dX_i^\eta}{d\tau} = 0; \quad (3.2)$$

the derivation of this boundary condition is given in Ref.[7]. For the perturbative boundary conditions, the weak-field solutions of Eqn.(2.16) are substituted into the system; the solutions are given in Ref.[4].

The technical details of the numerical work are not important, but a few general comments are in order on the practical aspects imposed by the boundary conditions and initial data.

Under both types of boundary conditions, the accuracy of the numerical results may be influenced by the length L of the string segment, meaning that if a string segment is too short, the motion of the boundary points induces incorrect behaviour. The larger the value of L , the smaller the effect, but the larger the value of L , the greater the number of grid points required to adequately resolve the string. The choice of string length is therefore a compromise between the need to accurately reproduce the behaviour of an infinite string and the need to use computing resources effectively. We found that the massive-particle boundary conditions required a string length of at least $L = 1000r_g$ to give reasonable results, as discussed in Ref. [7], whereas the perturbative boundary conditions required a much shorter string length, $L \sim 100r_g$, since the weak-field solutions represent the motion of the string boundary points with sufficient accuracy at these distances. Therefore, the perturbative boundary conditions greatly reduce the number of grid points and time steps needed to resolve the motion of the string near the black hole, and hence speed up execution dramatically.

Initial data takes the form of a straight string, Minkowski solution with the stipulation that the initial position of the string is sufficiently far away from the black hole to minimize the discrepancy between this approximate initial data and the correct initial configuration in Schwarzschild spacetime; the constraint equations are used as a guide. The constraint equations are also used to check the accuracy of the calculations during the time evolution of the string.

The evaluation of the discretized form of the constraint equations is carried out periodically during the numerical solution. Statistics are computed for the constraints (average value over the length of the string and standard deviation) at the current time step and reported to an output file. Monitoring that

the constraints are consistent with zero to several significant digits is done by inspecting this file. If the constraints are not satisfactorily maintained, that is if the average value grows unacceptably large or undergoes sudden changes, the numerical solution is restarted with new parameters (e.g. finer grid, finer step size). Typically, the constraints were expected to be consistent with zero to four significant figures for the perturbative version and six significant figures for the massive particle version. Tighter tolerances can be achieved by increasing the number of grid points (and significantly increasing solution time), but for the purposes of this study, the above values were deemed a reasonable compromise between accuracy and speed.

The perturbative solution to the equations of motion of an infinitely long cosmic string is most conveniently carried out in isotropic coordinates, (T, X, Y, Z) . Numerically, however, the scattering problem is best studied in Eddington-Finkelstein In-going coordinates since the Christoffel symbols in this coordinate system are regular everywhere. The Christoffel symbols associated with this coordinate system, along with their derivatives with respect to the spacetime coordinates, were derived and inserted as analytic expressions in the portions of the code dealing with the initialization of the tridiagonal matrices. Also, the coded forms of the analytic expressions for the initial data and for the perturbative boundary conditions were converted to Eddington-Finkelstein coordinates using standard coordinate transformations.

3.2 Scattering at intermediate velocities

In this section, we compare the numerical solutions of string scattering to those of the weak-field approximation at intermediate velocities ($0.1 < v/c < 1$) for a range of impact parameters. Our basis for comparison is the scattering data.

Figure 2 shows sections of the numerical worldsheet of a string with initial velocity $0.76c$ and impact parameter $40r_g$. As shown in Table 1, the maximum amplitude and width of the pulses is in good agreement with the weak-field Eqns. (2.23) and (2.24).

Table 1: Scattering data - Schwarzschild weak-field.

| | numerical | perturbation |
|----------------------------------|-----------|--------------|
| A_∞ | $3.4 r_g$ | $3.6 r_g$ |
| w | $140r_g$ | $165r_g$ |
| $(v = 0.76 c, \quad b = 40 r_g)$ | | |

When the impact parameter approaches the critical value for capture, the string is in a regime where

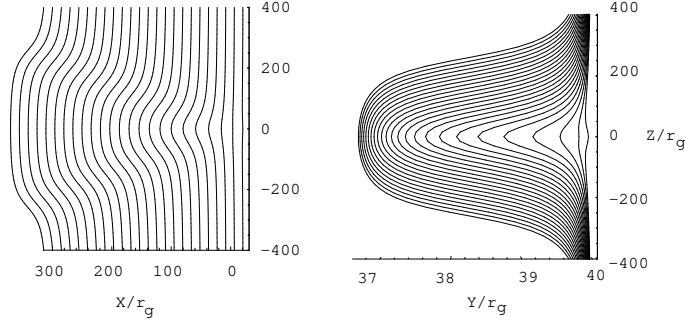


Figure 2: Time sequence of string scattering in weak-field regime (numerical results). Black hole lies at origin of coordinate system. Initial velocity $0.76c$, impact parameter $40 r_g$.

only numerical solutions are available. Figure 3 shows sections of the worldsheet of a slow string ($v = 0.2c$) with near-critical impact parameter ($b = 2.5 r_g$ compared to $b_{\text{capture}} = 2.1 r_g$). As shown in Table 2, the maximum amplitude of the pulses is considerably greater than predicted by weak-field Eqn. (2.23), while there is good agreement in terms of the measured width of the kink and Eqn. (2.24).

Table 2: Scattering data - Schwarzschild strong-field.

| | numerical | perturbation |
|-----------------------------------|-----------|--------------|
| A_∞ | $1.8 r_g$ | $0.95 r_g$ |
| w | $28 r_g$ | $27 r_g$ |
| $(v = 0.29 c, \quad b = 2.5 r_g)$ | | |

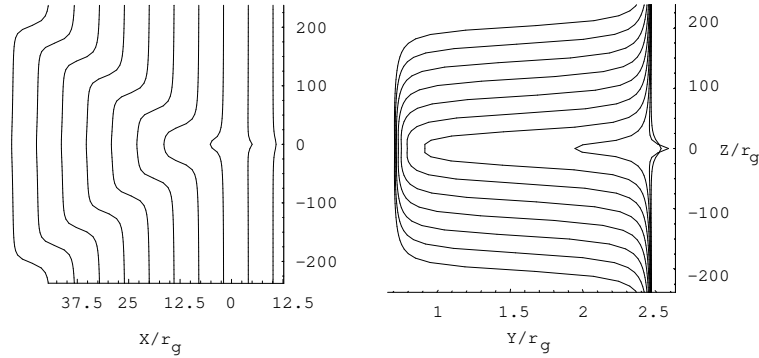


Figure 3: Time sequence of string scattering in strong-field regime (numerical results). Black hole lies at origin of coordinate system. Initial velocity, $0.29c$, impact parameter $2.5 r_g$.

It is important to note that, although the behaviour of the string is qualitatively consistent with the weak-field solutions, the total deflection of the string is greater than predicted by Eqn. (2.23). The discrepancy is made clear by plotting the total deflection of the string obtained from the numerical solver and comparing it to the prediction of Eqn. (2.23). This is done in Fig. 4, where the ratio $A_{\text{numerical}}/A_{\text{weak}}$

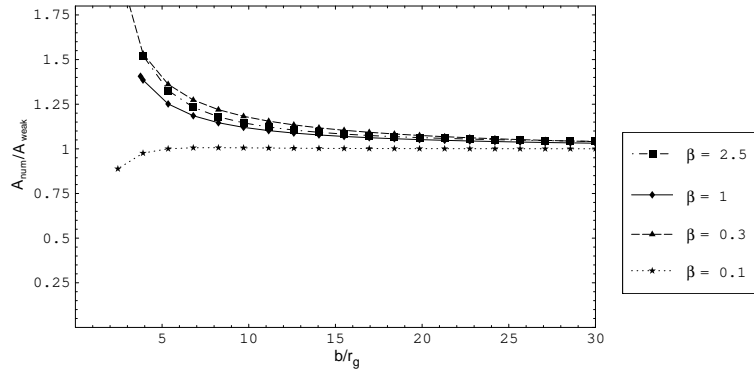


Figure 4: Comparison of numerical scattering data with weak-field approximation.

is plotted for four velocities. It can be seen that numerical and perturbative results converge for large impact parameters, and that the transition from weak-field to strong-field occurs for impact parameters on the order of $10 r_g$. Conversely, the curves make it clear that the weak-field solutions are quite acceptable down to very small impact parameters. The curve which suffers a downturn is the lower velocity one, meaning that Eqn. (2.23) predicts a greater shift than the numerical data. The velocity of the string in this case is at the upper threshold where second-order corrections to the perturbative expansion become important. Recall that the expression (2.23) was derived using results from first-order perturbative calculations.

4 Ultra-relativistic Limit and Loop Formation

4.1 Analytical results for ultra-relativistic scattering

In this section we consider scattering of a straight cosmic string by a black hole in the limit where the initial velocity is close to the velocity of light. Numerical studies of the evolution of stochastic networks of cosmic strings from initial formation to the matter era [8] suggest that astrophysical cosmic strings are expected to move with an average velocity $v \approx 0.7c$. For this reason, the results discussed in this section concerning motion at the ultra-relativistic limit are mainly of theoretical interest. Nevertheless, they provide a number of analytic expressions against which to validate numerical solutions in this regime.

In the limit $v \rightarrow c$, the gravitational field of a black hole in the reference frame of the string takes the form of a shock wave. The corresponding Aichelburg-Sexl metric [10] is of the form (see Appendix)

$$ds^2 = -dX_- dX_+ + dY^2 + dZ^2 - 4\gamma M F \delta(X_+) dX_+^2, \quad (4.1)$$

where $F = \ln \rho^2$, and $\gamma = (1 - v^2)^{-1/2}$. In these null coordinates, the initial motion of the straight string

is given by

$$X_+|_{\tau < 0} = \tau, \quad (4.2)$$

$$X_-|_{\tau < 0} = \tau - 2\gamma X_0, \quad (4.3)$$

$$Y|_{\tau < 0} = Y_0, \quad (4.4)$$

and

$$Z|_{\tau < 0} = \sigma. \quad (4.5)$$

The problem of scattering of the string in the metric (4.1) was studied earlier (see e.g. [11]). For our case, the corresponding solutions are (details in the Appendix)

$$X_+ = \tau, \quad (4.6)$$

$$X_-|_{\tau > 0} = \tau - 2\gamma X_0 - \gamma M \left[\ln(Y_0^2 + (\tau + \sigma)^2) + \ln(Y_0^2 + (\tau - \sigma)^2) \right], \quad (4.7)$$

$$Y|_{\tau > 0} = Y_0 - 2\gamma M \left[\arctan\left(\frac{\tau + \sigma}{Y_0}\right) + \arctan\left(\frac{\tau - \sigma}{Y_0}\right) \right], \quad (4.8)$$

and

$$Z|_{\tau > 0} = \sigma - \gamma M \ln \left[\frac{Y_0^2 + (\tau + \sigma)^2}{Y_0^2 + (\tau - \sigma)^2} \right]. \quad (4.9)$$

These results allow one to easily determine the amplitude of the kinks for the ultra-relativistic solutions. The maximum amplitude comes from the asymptotic value of $Y|_{\tilde{\tau} > 0}$,

$$A_\infty := Y_0 - \lim_{\tilde{\tau} \rightarrow \infty} Y|_{\tilde{\tau} > 0} = -2\pi \gamma M. \quad (4.10)$$

This result is in agreement with the result of weak field approximation (2.23), in the limit $v \rightarrow c$.

4.2 Loop formation

The formation of loops characterises ultra-relativistic scattering. A loop-like configuration appears when $Z(\tau, \sigma)$ is no longer a monotonic function of σ for a fixed value of τ . This occurs when $Z_{,\sigma} < 0$. From Eqn. (4.6), one gets

$$Z_{,\sigma} = 1 - 2\gamma M \left[\frac{\zeta_+}{Y_0^2 + \zeta_+^2} + \frac{\zeta_-}{Y_0^2 + \zeta_-^2} \right], \quad (4.11)$$

where $\zeta_{\pm} = \tau \pm \sigma$. The function $Z_{,\sigma}$ has extrema at $|\zeta_{\pm}| = |Y_0|$. The minimum of $Z_{,\sigma}$ occurs at $\zeta_+ = \zeta_- = Y_0$, that is at $\tau = Y_0$ and $\sigma = 0$. This minimal value $Z_{,\sigma} = 1 - 2\gamma M/Y_0$ becomes negative when

$$2\gamma M > Y_0. \quad (4.12)$$

This is the condition for loop formation. This condition can be overlaid on the capture curve [7], as shown in Fig. 5. The loop formation region lies above the capture curve and to the right of the curve $\gamma = Y_0/r_g$; it can be seen that loop formation is a relativistic phenomenon, and the ultra-relativistic solution predicts that this effect cuts off for velocities below $v \sim 0.9c$

The maximum width of the loops, w_{loop} , occurs when the solution for $Z|_{\tilde{\tau}>0}$ reaches an extremum in both τ and σ . It is straightforward to compute the derivatives from Eqn. (4.6) and show that

$$w_{loop} = 2\gamma \left\{ \eta - \frac{1}{2} \ln \left[\frac{1+\eta}{1-\eta} \right] \right\} (r_g) \quad ; \quad \eta = \sqrt{1 - \left(\frac{Y_0}{2M\gamma} \right)^2}. \quad (4.13)$$

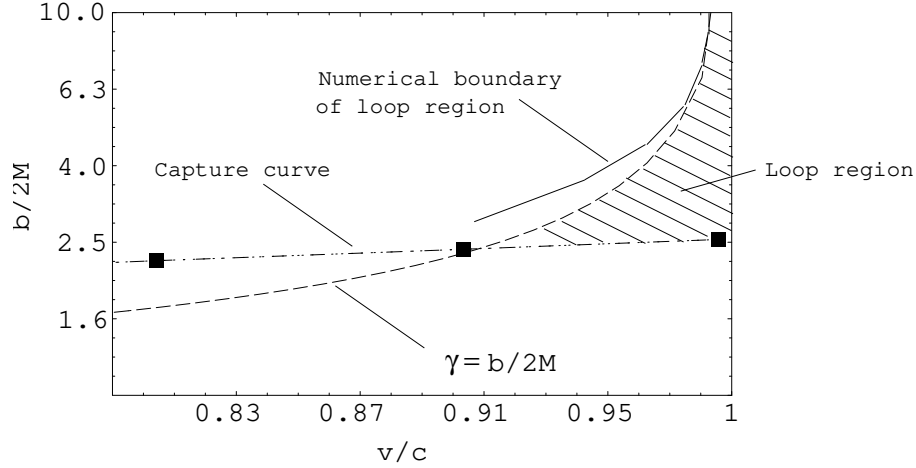


Figure 5: Loop formation region.

4.3 String self-intersection

The formation of loops is accompanied by string self-intersection. Self-intersection occurs if there exists a pair of points on the string worldsheet, (τ_1, σ_1) and (τ_2, σ_2) , such that

$$\mathcal{X}^\mu(\tau_1, \sigma_1) = \mathcal{X}^\mu(\tau_2, \sigma_2). \quad (4.14)$$

Since this condition forms a system of 4 equations for 4 variables, in the general case the self-intersection points are isolated. For the highly symmetric initial-value problem used here, a point of self-intersection

is located at $Z = 0$. Let

$$F(\zeta) = \zeta - 2\gamma M \ln(Y_0^2 + \zeta^2), \quad (4.15)$$

then $Z = 0$ when $F(\zeta_+) = F(\zeta_-)$. This condition is satisfied for two different points $(\zeta_{+,1}, \zeta_{-,1})$ and $(\zeta_{+,2}, \zeta_{-,2})$ if and only if there exist two different values of c (say, c_1 and $c_2 > c_1$) such that $F(c_1) = F(c_2)$. It happens when the function F is non-monotonic, and the equation

$$F'(\zeta) = 1 - 2\gamma M \zeta / (Y_0^2 + \zeta^2) = 0 \quad (4.16)$$

has a solution. The latter condition implies $2\gamma M \geq Y_0$. This is exactly the same condition of loop formation which was obtained earlier, Eqn. (4.12). The equation $F(c_1) = F(c_2)$ has solutions for

$$c_1 \in (2\gamma M - \sqrt{4(\gamma M)^2 - Y_0^2}, 2\gamma M + \sqrt{4(\gamma M)^2 - Y_0^2}). \quad (4.17)$$

It is easy to verify that for such c_1 all the conditions of self-intersection are met if $\zeta_{-,1} = c_1$, $\zeta_{+,1} = c_2$, $\zeta_{-,2} = c_2$, and $\zeta_{+,2} = c_1$. Simple analysis shows that the self-intersection is stable with respect to small perturbations of the initial state of the string before its scattering by the black hole.

4.4 Numerical results

Figure 6 shows sections of the numerical worldsheet of a string propagating with an initial velocity of $0.995c$ ($\gamma = 10$) and impact parameter of $4r_g$. The view looking down onto the XZ plane show a complicated early phase associated with the evolution of short-lived loops and, at late times, two kink-like pulses propagating outward. The speed of the pulses is again that of light. The projections onto the YZ plane shows more clearly the early evolution of the loops, which indicate that the points on the string near the $Z = 0$ plane undergo a short-lived deflection across the $Z = 0$ plane. The formation of loops suggests that the behaviour of the string at periastron is particle-like in that there is insufficient time for tension to play a role, and the points on the string undergo a temporary Keplerian deflection. However, once clear of the black hole, the tension can again assert itself and solitonic pulses with an S-shaped profile emerge and propagate outward. Figure 6 also shows that the string self-intersects in the $Z = 0$ plane. As the loop grows, the intersection point moves gradually downward in the Y-direction. Once the loop has reached its maximum size, the S-shaped kinks have formed and begin to propagate outward, away from the $Z = 0$ plane. The intersection point disappears when the kinks have completely separated.

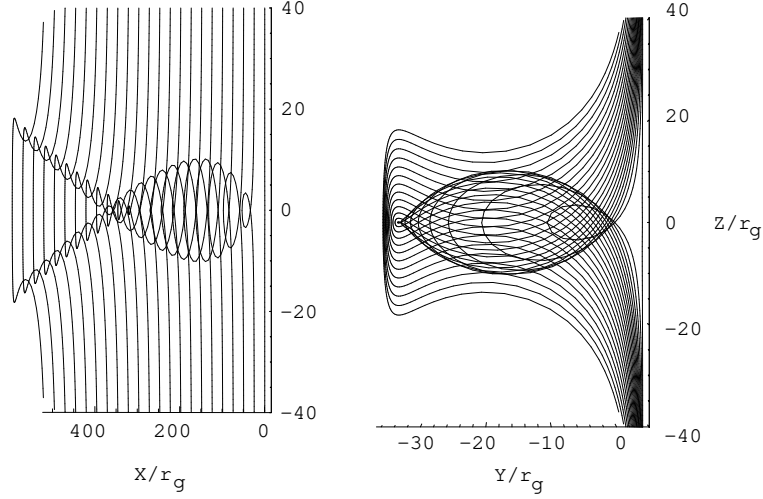


Figure 6: Time sequence of string scattering in ultra-relativistic regime (numerical results). Black hole lies at origin of coordinate system. Initial velocity $0.995c$, impact parameter $4.0 r_g$.

Figure 7 shows YZ sections generated from the analytic weak-field and ultra-relativistic solutions for the same physical parameters and intervals of proper time as in Fig. 6. The two analytic solutions are virtually indistinguishable, the only difference being in the first slice, taken at the time where the string reaches periastron. The ultra-relativistic solution shows a completely straight string, as expected, since the black hole does not begin to distort the string until it has passed over it. The weak-field solution shows a slightly bent string, indicating that even at $0.995c$, the influence of the black hole is felt before closest approach. For later times, the two solutions are indistinguishable.

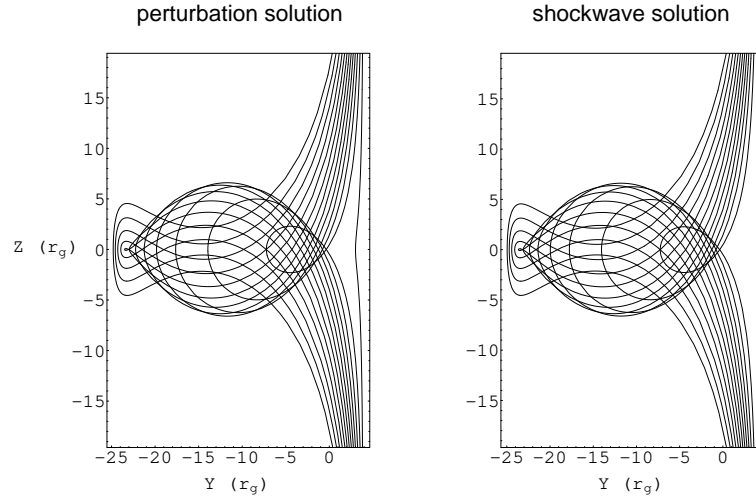


Figure 7: Time sequence of string scattering in ultra-relativistic regime (analytic). Black hole lies at origin of coordinate system. Initial velocity, $0.995c$, impact parameter $4.0 r_g$.

As shown in Table 3, the maximum amplitude of the deflection and the size of the loops in the

numerical data is slightly larger than predicted by Eqns. (4.14) and (4.17). It is important to note that $\gamma = 10$ for these figures, which is low for the ultra-relativistic approximation, but represents a practical upper bound for numerical computations³. Furthermore, the impact parameter is very small, and, as shown in the previous section, the approximate solutions are no longer completely accurate under these circumstances.

Table 3: Scattering data - Schwarzschild ultra-relativistic.

| | numerical | perturbation |
|------------------------------------|-----------|--------------|
| A_∞ | $40 r_g$ | $31.6 r_g$ |
| w_{loop} | $20 r_g$ | $13.2 r_g$ |
| $(v = 0.995 c, \quad b = 4.0 r_g)$ | | |

Since the weak-field and ultra-relativistic approximations are accurate only for impact parameters greater than $\sim 10r_g$, the boundary of the loop formation is expected to shift due to strong field effects. The solid line shown in Figure 5, based on numerical tests to detect loop formation, indicates that the boundary is shifted towards lower velocities; the strong field near the black hole tends to enhance loop formation⁴.

The black hole drives the self-intersection process as its gravitational influence draws points on either side of the string towards the $Z = 0$ plane. The string model used here does not allow for the string to break at the self-intersection point. Where such models have been discussed (see, e.g., [8] and [12]), it is thought that a loop formed through self-intersection would break off and the remaining segments of string would reconnect. The size of such loops is thought to be small. If this is indeed the case, then the black hole driven self-intersection could leave a line of small loops in the wake of the string, yielding a physical picture far different from the one shown here. How each of these loops would then interact with the black hole would also prove an interesting problem.

³This is due to numerical anomalies that develop when larger γ -factors are considered. These numerical anomalies manifest themselves as a rigid deflection of the entire string as it crosses the $X = 0$ plane. The cause of these anomalies was traced to a loss of resolution in the first-order angular derivatives $\partial_\phi \mathcal{X}^\mu$ at large γ -factors. The problem is suppressed by increasing the number of grid points; the large grid sizes required result in a numerically intensive solver.

⁴Our numerical results are inconsistent with the findings of Lonsdale and Moss[6], who observe loops at much lower velocities and larger impact parameters.

5 Near-critical Scattering

As we already mentioned, there are two possible outcomes when a cosmic string interacts with a black hole: either the string is scattered, or it is captured by the black hole. For a given initial velocity v the outcome depends on the value of the impact parameter b . In other words, in the space of initial data (v, b) there exists a critical line $b = b_{crit}(v)$ which separates these two different regimes. We discuss the critical impact parameter for string capture in Section 7. This section discusses string scattering where the impact parameter is extremely close to the critical impact parameter for capture and the string comes close to the black hole. In a similar situation for test particle scattering, the particle can execute multiple orbits around the black hole before escaping. Some similarities with particle scattering are observed, but there are also important differences that shed light on the process of string capture.

Figure 8 compares a slice of the string worldsheet through the $Z = 0$ plane to the motion of a test particle. A comparison is made of a series of string and particle trajectories with identical velocities ($v = 0.987c$) and nearly identical impact parameters. For the particle trajectories, these range from $b = 2.60 r_g$ through $b = 2.65 r_g$. For the string, the impact parameters are slightly smaller, ranging from $b = 2.55 r_g$ through $b = 2.56 r_g$. The impact parameters at the lower end of each range result in capture, whereas those at the upper end result in scattering. It is easy to see that, even at ultra-relativistic velocities, tension influences string motion. Although the critical impact parameter for the string is very close to that for a particle, suggesting that tension plays a limited role, the dynamics of the string are, nevertheless, still governed by tension. This is made especially clear by the folded appearance of the escaping string trajectories. The escaping trajectories of the test particle are far less complicated.

The detailed motion of the string in the critical regime close to capture is highly sensitive to the initial impact parameter. Figure 8 shows that there are two types of capture trajectories, trajectories such as curve 1, where the string crosses the horizon directly, and curve 2, where the string folds back on itself before crossing the horizon. Curve 2 exhibits a loop-like feature, but does not represent a self-intersection since the intersecting points have distinct proper times. Escaping trajectories, such as curve 3, have a folded structure. There are two critical cases that mark the transition between each of these three generic curves. The transition between curves of type 1 and type 2 is marked by a structure that develops an increasingly cusp-like shape (point B in Fig. 8) as the impact parameter approaches the critical value that marks the transition from type 1 to type 2 curves. In practical terms, this impact parameter is difficult to obtain since it requires a large number of significant digits (curve 1 and the curve with point B have

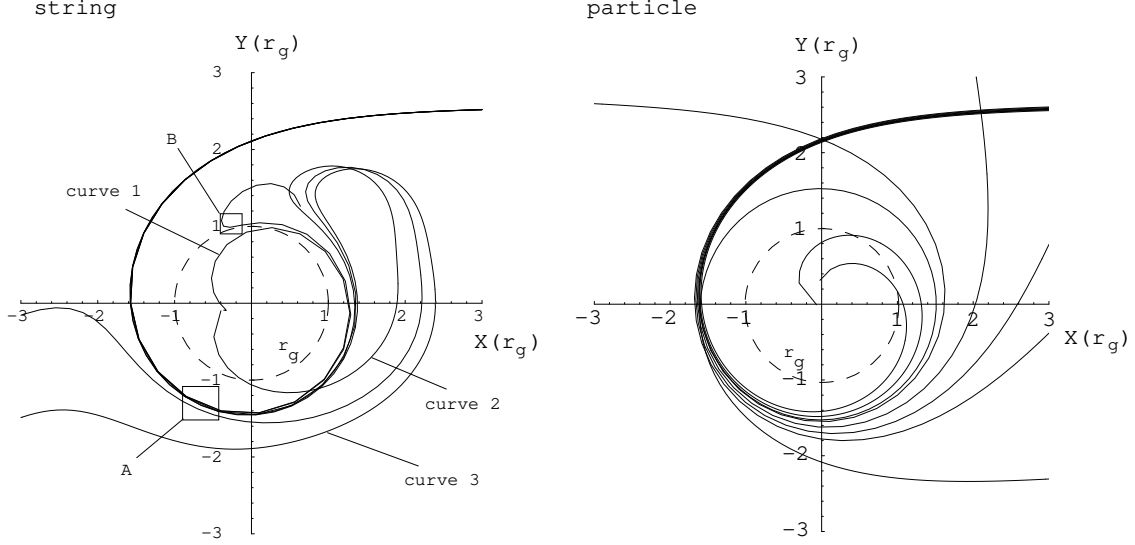


Figure 8: Near-critical scattering for string and test particle; $v = 0.987c$ and $r_g = 1$.

impact parameters that differ by one part in 10^5). The transition between type 2 and type 3 curves is marked by a tangent point, where the string trajectory passes twice through the same point (point A) at different times (again, no self-intersection). Furthermore, the transition between type 2 and type 3 curves is associated with the critical impact parameter for capture.

A full 3D rendering of the worldsheet nearest the black hole can be generated, but it is very difficult to interpret and is therefore not shown here. It is sufficient to note that complicated folds and twists are generated as points on the string cross and recross while executing their partial orbit of the black hole. At late times, however, these folds and twists have dissipated and all that remains are kinks, as shown in Fig. 9. This Figure reinforces the idea that scattering at late times is completely understood in terms of the perturbative solutions. However, it may take a significant amount of time for the simple kink/anti-kink picture to emerge. In the case studied here, the distortions due to the close encounter persist until the string is about $1000 r_g$ past the black hole.

The numerical results for moderate γ -factors show that the string worldsheet folds back on itself, with no evidence of multiple windings or glory scattering as would be the case for near-critical scattering of particles. In fact, it seems as if the transition to a "direct capture" trajectory (like curve 1 in Fig. 8) always occurs before a full turn is achieved. The fact that multiple windings are absent is a clear indication that the tension in remote parts of the string eventually asserts itself in all cases accessible to the numerical solver. The question as to whether the string can complete more than one full turn and "wrap" the black hole for larger γ -factors is an open one.

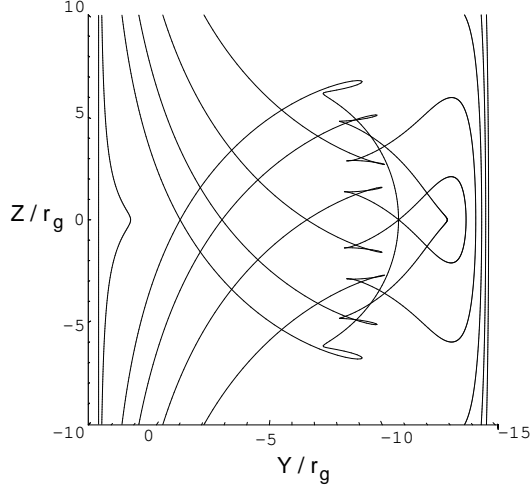


Figure 9: String worldsheet at late proper time, $v = 0.987c$. Loops dissipate and kinks emerge.

6 Role of String Tension - Dust Strings

Since a cosmic string is an extended object under tension, motion of a string near a black hole represents the result of the competing influences of tension and gravity. In order to shed light on the role of tension in the dynamics of the string, the motion of the string is compared to the motion of an array of test particles initially configured with the same position and initial velocity as the cosmic string. To do this, consider a family of N test particles arrayed on a line with initial position $\mathcal{X}^\mu_i(\tau_0)$ and initial velocity $\partial_\tau \mathcal{X}^\mu_i(\tau_0)$, where i is a position index (an integer between 1 and N) that describes the initial location of the test particle on the line. These particles each satisfy the geodesic equation and constraint,

$$\begin{aligned} \frac{d^2 \mathcal{X}^\nu_i}{d\tau^2} + \Gamma^\nu_{\rho\sigma} \frac{d\mathcal{X}^\rho_i}{d\tau} \frac{d\mathcal{X}^\sigma_i}{d\tau} &= 0, \\ \frac{d}{d\tau} \left[g_{\mu\nu} \frac{d\mathcal{X}^\mu_i}{d\tau} \frac{d\mathcal{X}^\nu_i}{d\tau} \right] &= 0. \end{aligned} \quad (6.1)$$

It is easy to show that, in flat spacetime,

$$X^\mu_i(\tau) = (\cosh(\beta)\tau, \sinh(\beta)\tau + X_0, Y_0, \sigma_i) \quad (6.2)$$

satisfies these equations and represents a straight dust string moving with velocity $v = \tanh \beta$ where the discrete σ_i mimic the σ coordinate of the cosmic string.

In the weak-field and ultra-relativistic cases, the role of tension in the string is made apparent by comparing the YZ projections of Figs. 2 and 5 against those of the dust string in Fig. 10. Figure 10 shows that a loop always evolves in the dust string worldsheet. This loop is due to the Keplerian nature of the trajectories of each particle on the dust string. Particles lying on one side of the $Z = 0$ plane are

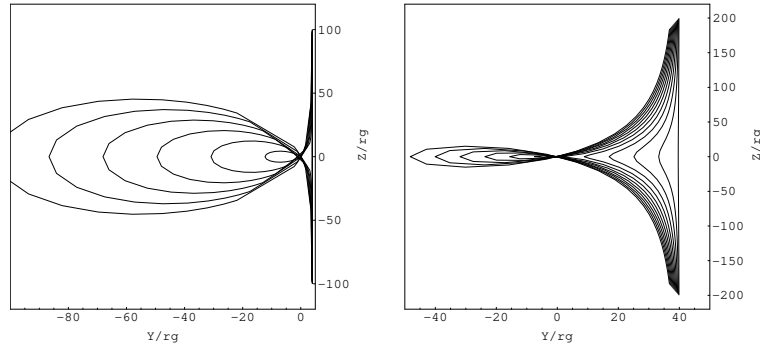


Figure 10: Time sequence of dust string scattering in ultra-relativistic regime. Black hole lies at origin of coordinate system. Left: Initial velocity $0.995c$, impact parameter $4.0 r_g$. Right: Initial velocity $0.76c$, impact parameter $40 r_g$.

deflected across this plane since their motion is constrained to an orbital plane passing through the black hole. Unlike the cosmic string, the Y-axis deflection of the dust string is unbounded (this is not to say that the deflection does not reach an asymptotic angular value). Close examination of Figs. 2, 5, and 10 reveals that, at the early stages of scattering, the size of the loops in the dust and cosmic strings are virtually identical, reinforcing the idea that tension takes some time to assert itself. Loop formation is a generic feature of the dust string; this is not the case for the cosmic string, where loop formation is subject to the low-velocity cut-off effect discussed above.

In the strong-field regime (with $v < c$), a comparison to the dust solution is uninformative since the impact parameter is well below the critical value for particles and the portion of the dust string near the equatorial plane is captured by the black hole. However, it does reinforce the idea that internal tension plays an important role in the dynamics of the string, helping the string avoid capture for impact parameters well below that of the dust string.

7 String Capture

In Ref. [7] we presented a plot of the critical impact parameter for capture as a function of velocity, the capture curve for cosmic strings. In that paper, we used the massive-particle boundary conditions exclusively and showed that, for string lengths greater than $2000r_g$, the capture curve was definitive for velocities greater than $0.2c$. We are now in a position to revisit this curve using the perturbative boundary conditions in the improved numerical solver, and to merge the numerical findings with the ultra-low velocity results of [4] to present a complete capture curve.

The revised capture curve shown in Figure 11 validates two claims made in the previous paper. First, that the capture curve for long strings is indeed definitive (provided focusing of end points is negligible).

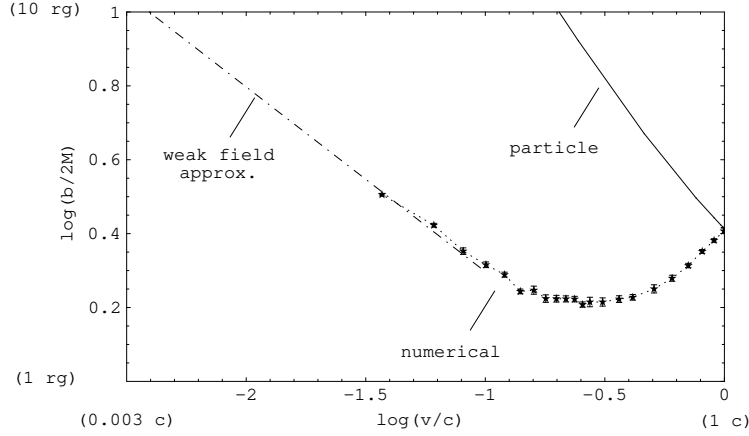


Figure 11: Cosmic string capture curve for Schwarzschild black hole - data from numerical and perturbative results.

This is so because the revised capture curve is identical to that of the $L = 2000 r_g$ string for $v > 0.2c$. Second, that there is indeed a minimum impact parameter at intermediate velocities, which occurs at $v \approx 0.2c$ and has a value of $1.6 r_g$. However, it is important to note that the new solver is also velocity-limited in that, at sufficiently low velocities, second-order perturbative effects become important and invalidate the first-order solutions used to set the boundary conditions. Nevertheless, analytic results [4, 5] are available for this velocity range, and the numerical results join smoothly with the analytical result for the critical impact parameter for very low velocities

$$b_{\text{capture}} \sim \frac{r_g}{2} \sqrt{\frac{\pi}{2v}}, \quad (7.1)$$

and is shown as a dashed line in Fig. 11. This capture curve also is in a good agreement with a recent result by Page [5] for the critical impact parameter,

$$b_{\text{capture}} \sim \frac{r_g}{2} \left[\sqrt{\frac{\pi}{2v}} - \left(\sqrt{\frac{\pi}{2}} + \frac{64}{15} - \sqrt{27} \right) + \frac{64}{15} v \right]. \quad (7.2)$$

This formula reproduces the general shape of the curve shown in Fig. 11, without the fine structure that is revealed by the numerical approach. The error bars ⁵ in Fig. 11 are quite small. With such tight values for critical impact parameter, it is quite apparent that the capture curve is not a smooth line, but has some fine structure to it. This has to do with the complicated nature of the trajectory of the string for near-critical impact parameters.

It should be emphasized that our numerical results demonstrate that in the limit $v \rightarrow c$ the critical impact parameter reaches the same value, $3\sqrt{3}GM/c^2$, as the critical impact parameter for capture of

⁵As defined in [7], the lower error bar denotes the largest impact parameter resulting in capture and the upper error bar denotes the smallest impact parameter resulting in escape for a given initial velocity.

ultrarelativistic particles. This result is inconsistent with the earlier results of Moss and Lonsdale [6]. Moreover, the analytical result (7.1) also is inconsistent with the results of Moss and Lonsdale, who quote a low-velocity dependence of v^{-1} obtained from a numerical fit to their capture curve.

8 Conclusions

In this paper, we discussed the gravitational scattering of cosmic strings by Schwarzschild black holes. This paper brought together earlier results for the critical impact parameter for capture, weak-field analytic solutions, and studied the limitations of approximate solutions as a function of velocity and impact parameter by generating numerical solutions to the equations of motion. Earlier findings have been corroborated by these latest results, and numerical, weak-field, and shockwave results are consistent with one another in the regions where they overlap.

The scattering problem was studied in three regimes. In the ultra-relativistic regime, we showed that strings form loops, provided that the conditions $Y_0 \leq 2\gamma M$ and $Y_0 > b_{capture}$ are satisfied; this phenomenon cuts off for velocities below $\sim 0.9c$. A detailed comparison of analytic and numerical results showed that the perturbative results break down for $Y_0 < 10r_g$; this is a surprisingly small value and suggests that the weak-field approximation is quite acceptable for all cases except near-critical scattering. Where the weak-field approximation breaks down, in the strong-field regime, kinks are produced (without loops for $v < 0.9c$, with loops for $v > 0.9c$), but their amplitude is larger than predicted by approximate solutions.

In the case of near-critical scattering, the string worldsheet evolves highly complicated structures. A detailed investigation of string motion in this case showed that there are two characteristic trajectories for capture, the first where the string enters directly, the second where the string evolves a small loop before crossing the horizon. This complicated behaviour, and its extreme sensitivity to initial data, explain the structure observed in the capture curve.

This paper has also shown the critical role performed by tension in determining the dynamics of the string. The absence of multiple string windings around the black hole and the complicated folds observed in the string worldsheet at near-critical scattering, even at moderate γ -factors, suggest that internal tension plays an important role in scattering.

Acknowledgments: This work was partly supported by the Natural Sciences and Engineering Research Council of Canada. One of the authors (V.F.) is grateful to the Killam Trust for its financial

support. The authors are also grateful to Don Page for numerous discussions.

Appendix - Analytical Results in Shockwave Regime

In this Appendix we present a solution for an ultra-relativistic straight string scattered by a black hole. The key observation which leads to a solution of the equations of motion in the ultra-relativistic limit is the following: in the reference frame of the string the black hole moves with $v \approx 1$ and its gravitational field is boosted to the shock wave [13]. As a result, before and after crossing the null surface N representing the black hole, the string obeys the free equations in flat spacetime. All the information concerning the non-linear interaction with the gravitational field of the black hole can be obtained in the form of “jump” conditions on the null surface N . Such solutions were studied earlier (see e.g. Ref. [11]).

To obtain the metric of an ultra-relativistic black hole one starts with the metric (2.10) written in the form

$$ds^2 = (1 + 2\Psi)ds_0^2 + 2(\Phi + \Psi)dT^2, \quad (\text{A.1})$$

where

$$ds_0^2 = -dT^2 + dX^2 + dY^2 + dZ^2, \quad (\text{A.2})$$

and make the boost transformation

$$\bar{T} = \gamma(T - vX), \quad \bar{X} = \gamma(X - vT), \quad \bar{Y} = Y, \quad \bar{Z} = Z. \quad (\text{A.3})$$

Let $X_{\pm} = \bar{T} \pm \bar{X}$ so that

$$X_+ = \gamma(1 - v)(T + X), \quad X_- = \gamma(1 + v)(T - X), \quad (\text{A.4})$$

and, since $\gamma^2 = (1 - v^2)^{-1}$,

$$\begin{aligned} T &= \frac{\gamma}{2}(1 + v) \left(X_+ + \left(\frac{1 - v}{1 + v} \right) X_- \right), \\ X &= \frac{\gamma}{2}(1 + v) \left(X_+ - \left(\frac{1 - v}{1 + v} \right) X_- \right). \end{aligned} \quad (\text{A.5})$$

Using Eqns. (A.5) the metric (A.1) takes the form

$$\begin{aligned} ds^2 &= (1 + 2\Psi) [-dX_- dX_+ + dY^2 + dZ^2] \\ &+ \frac{\gamma^2}{2}(1 + v)^2(\Phi + \Psi) \left(dX_+ + \frac{1 - v}{1 + v} dX_- \right)^2. \end{aligned} \quad (\text{A.6})$$

In the lowest order $\Phi = \Psi = \varphi = M/R$, where $R = \sqrt{X^2 + Y^2 + Z^2}$ can be rewritten using Eqn. (A.5)

as

$$R = \gamma \sqrt{\left(\frac{1+v}{2}\right)^2 \left(X_+ - \left(\frac{1-v}{1+v}\right) X_+\right)^2 + \frac{1}{\gamma^2} (Y^2 + Z^2)} \quad (\text{A.7})$$

so that

$$\varphi = \frac{\gamma M (1-v^2)}{\left[\left(\frac{1+v}{2}\right)^2 \left(X_+ - \left(\frac{1-v}{1+v}\right) X_+\right)^2 + (1-v^2)(Y^2 + Z^2)\right]^{1/2}}. \quad (\text{A.8})$$

The metric (A.6) takes the form

$$\begin{aligned} ds^2 = & -dX_- dX_+ + dY^2 + dZ^2 \\ & + 2\varphi (dY^2 + dZ^2) + \gamma^2 \varphi \left((1+v)^2 dX_+^2 + (1-v)^2 dX_-^2\right) \end{aligned} \quad (\text{A.9})$$

In the limit $v \rightarrow 1$ and γM fixed one has [11]

$$\lim_{v \rightarrow 1} \gamma^2 \varphi = \lim_{v \rightarrow 1} \frac{\gamma M}{\sqrt{X_+^2 + (1-v^2)\rho^2}} = -\gamma M \delta(X_+) \ln \rho^2, \quad (\text{A.10})$$

where $\rho^2 = Y^2 + Z^2$. From this it follows that the metric in the Aichelburg-Sexl form [10] is obtained

$$ds^2 = -dX_- dX_+ + dY^2 + dZ^2 - 4\gamma M F \delta(X_+) dX_+^2. \quad (\text{A.11})$$

where $F = \ln \rho^2$. The boosted metric in this form represents a gravitational shockwave. The following components of the Christoffel symbols do not vanish:

$$\begin{aligned} \Gamma_{++}^- &= 4\gamma M F \delta'(X_+), \quad \Gamma_{+Y}^- = 2\Gamma_{++}^Y = 4\gamma M F_{,Y} \delta(X_+), \\ \Gamma_{+Z}^- &= 2\Gamma_{++}^Z = 4\gamma M F_{,Z} \delta(X_+). \end{aligned} \quad (\text{A.12})$$

The in-coming straight string motion (2.5) in this limit takes the form

$$X_+|_{\tau < 0} = \tau, \quad X_-|_{\tau < 0} = \tau - 2\gamma X_0, \quad Y|_{\tau < 0} = Y_0, \quad Z|_{\tau < 0} = \sigma. \quad (\text{A.13})$$

First solve the string equation (2.3) in the metric (A.11) for the initial conditions (A.13) using the conformal gauge in which $\sqrt{-h}h^{AB} = \eta^{AB}$, so that $\square = -\partial_\tau^2 + \partial_\sigma^2$.

The equation for X_+ takes a simple form

$$\square X_+ = 0. \quad (\text{A.14})$$

Hence its solution obeying the proper initial conditions is

$$X_+ = \tau. \quad (\text{A.15})$$

The equation for Y is

$$\square Y = 2\gamma M F_{,Y} \delta(\tau). \quad (\text{A.16})$$

The solution obeying the initial conditions (A.13) is solved using Green's Function methods [4] and has the form

$$Y|_{\tau>0} = Y_0 - 2\gamma M \left[\arctan\left(\frac{\tau + \sigma}{Y_0}\right) + \arctan\left(\frac{\tau - \sigma}{Y_0}\right) \right]. \quad (\text{A.17})$$

Similarly, solving equation

$$\square Z = 2\gamma M F_{,Z} \delta(\tau) \quad (\text{A.18})$$

for Z with the initial conditions (A.13) one gets

$$Z|_{\tau>0} = \sigma - \gamma M \ln \left[\frac{Y_0^2 + (\tau + \sigma)^2}{Y_0^2 + (\tau - \sigma)^2} \right]. \quad (\text{A.19})$$

And finally, a solution of the equation for X_-

$$\square X_- = 4\gamma M F \delta'(\tau) \quad (\text{A.20})$$

is

$$X_-|_{\tau>0} = \tau - 2\gamma X_0 - \gamma M \left[\ln(Y_0^2 + (\tau + \sigma)^2) + \ln(Y_0^2 + (\tau - \sigma)^2) \right]. \quad (\text{A.21})$$

It is easy to verify that the obtained solutions obey constraint equations (2.4) which for the case under consideration take the form

$$\dot{Y}^2 + Y'^2 + \dot{Z}^2 + Z'^2 = \dot{X}_- + 4\gamma M F \delta(\tau), \quad (\text{A.22})$$

$$\dot{Y}Y' + \dot{Z}Z' = \frac{1}{2}X'_-, \quad (\text{A.23})$$

Here a dot and prime denote derivatives with respect to τ and σ .

References

- [1] Frolov, V.P., Hendy, S., and Larsen, A.L. Phys. Rev. **D54**, 5093-5102 (1996).
- [2] Polyakov, A.M., Phys. Lett. **B103**, 207-210 (1981).
- [3] Frolov, V.P., Skarzhinsky, V.D., Zelnikov, A.I., and Heinrich, O. Phys. Lett. **B224**, 255 (1989).
- [4] De Villiers, J.P., and Frolov, V.P. Phys. Rev. **D58**, 105018(8) (1998).

- [5] Page, D.N. Phys. Rev. **D58**, 105026(13) (1998).
- [6] Lonsdale, S. and Moss, I. Nucl. Phys. **B298**, 693-700 (1988).
- [7] De Villiers, J.P., and Frolov, V.P. To appear in Int. J. Mod. Phys. **D7** No. 6 (December 1998).
- [8] Vilenkin, A. and Shellard, E. P. S., *Cosmic strings and other topological defects*. (Cambridge Univ. Press, Cambridge) (1994).
- [9] Misner, C.W., Thorne, K.S., and Wheeler, J.A. *Gravitation* (W.H. Freeman, San Francisco, 1973).
- [10] Aichelburg, P.C., and Sexl, R.U. Gen. Rel. Grav. **2**, 303-312 (1971).
- [11] Amati, D., and Klimcik, C. Phys. Lett. **B210** 92-96 (1988).
- [12] Albrecht, A. and York, T. Phys. Rev. **D38**, 2958-2962 (1988).
- [13] Hayashi, K., and Samura, T. Phys. Rev. **D50** 3666-3673 (1994).